Solar Energy Materials and Solar Cells 153, 124 (2016)

Light absorption enhancement for ultra-thin $Cu(In_{1-x}Ga_x)Se_2$ solar cells using closely packed 2-D SiO_2 nanosphere arrays

G. Yin[1*], P. Manley[1], M. Schmid[1,2]

[1]Helmholtz-Zentrum Berlin für Materialien und Energie GmbH, Nanooptische Konzepte für die PV, Hahn-Meitner Platz 1, 14109 Berlin, Germany

[2]Freie Universität Berlin, Fachbereich Physik, Arnimallee 14, 14195 Berlin, Germany

[*]Corresponding author: guanchao.yin@helmholtz-berlin.de (Guanchao Yin)

Tel: +49 30 806243721, fax: +49 30 806243199

Abstract: 2-D closely packed SiO_2 nanosphere arrays serving as the photonic structure for light absorption enhancement on top of ultra-thin $Cu(In_{1-x}Ga_x)Se_2$ solar cells are investigated both theoretically and experimentally. It is theoretically demonstrated that whispering gallery modes and high order Mie resonances contribute to the light absorption enhancement for the large spheres and an anti-reflection effect is prominent for small ones. The ultra-thin CIGSe solar cells achieve the optimum absorption enhancement for the small sphere array with a diameter of 110 nm, contrary to the larger spheres used in Si solar cells. The reason is attributed to the strong parasitic absorption in the AZO/ZnO/CdS front layers. They absorb mainly in the short wavelength range where the Mie resonances occur. Additionally, it is shown that the 110-nm-diameter sphere array exhibits a better angular tolerance than a conventional planar anti-reflection layer, which shows the potential as a promising anti-reflection structure.

Keywords: ultra-thin $Cu(In_{1-x}Ga_x)Se_2$ solar cells, closely packed SiO_2 nanosphere array, whispering gallery modes, Mie resonances, anti-reflection effect

1. Introduction

To increase the competitiveness of $Cu(In_{1-x}Ga_x)Se_2$ (CIGSe) solar cells and to obtain a large market deployment, further reduction of the cell manufacturing cost is desired. One approach to lower the cost is to reduce the thickness of the CIGSe photoactive layer, which allows for the reduction of material consumption, especially of the rare element In. However, reducing the thickness of the CIGSe photoactive layer from the typical 2-3 μm to below 500 nm will inevitably lead to incomplete absorption of the incident light and will deteriorate the solar cell performance [1-3]. Therefore, light absorption enhancement is crucial to maintaining high

efficiencies for ultra-thin (absorber thickness below to 500 nm) CIGSe solar cells. Previously, light absorption enhancement for CIGSe solar cells was achieved by coating an anti-reflection layer of MgF_2 [4, 5] or by improving the internal reflection at the CIGSe/Mo interface via inserting a dielectric layer [6] or via transferring the cells from the typical Mo back contact onto Au which has a better reflectivity [7]. Recently, a number of innovative nanoscale light-trapping structures have shown the potential to better improve the light absorption including plasmonic structures [8-11], dielectric diffractive nanostructures [12, 13] and photonic crystals [14, 15]. However, these innovative structures are mainly for Si-based, GaAs and organic solar cells, a few have been reported for CIGSe solar cells but were limited to theoretical investigations [16-18]. The reasons for the difficulty of experimental implementation are assumed to be: Firstly, CIGSe solar cells are mostly deposited on Mo back contact, which makes the implementation of light-trapping nanostructures hard underneath the back contact; secondly, CIGSe absorbers are normally prepared at a substrate temperature above 500 °C and this temperature can trigger the diffusion of plasmonic materials (Au, Ag) prepared before CIGSe deposition.

The 2-D dielectric sphere array is a promising structure for preparing nanostructures of other materials as a mask [19, 20] and light absorption enhancement in opto-electronic devices [15, 21-23]. Confined resonant modes can be supported when the size of spheres is on the scale of the wavelength. The energy in the resonant modes can leak into the solar cells if the spheres are placed in close proximity [15]. Additionally, the dielectric sphere arrays have other advantages [15, 19-24]: 1) dielectric materials are optically lossless, the concern of parasitic absorption is not necessary; 2) the geometry of the spheres is symmetric, which allows a broader acceptance angle of incident light; 3) the sphere array can be fabricated by the simple and cheap self-assembly method rather than complicated and expensive lithography technologies; 4) the inorganic dielectric materials are thermally stable compared to metallic materials, which makes them compatible to the deposition of the CIGSe layer at high substrate temperatures.

It has been implied that the 2-D colloidal SiO_2 sphere array on top of a thin-film solar cell can significantly improve the light absorption, which has been demonstrated in amorphous Si solar cells [21, 22]. However, since the structure and optical properties of CIGSe solar cells show a pronounced difference to Si solar cells, whether the 2-D colloidal SiO_2 sphere array can serve as an effective light-trapping structure for ultra-thin CIGSe solar cells is unknown.

In this work, we investigate the optical influence of the SiO_2 sphere arrays on top of ultra-thin CIGSe solar cells and identify the underlying mechanisms of light absorption enhancement.

2. Simulations and experiments

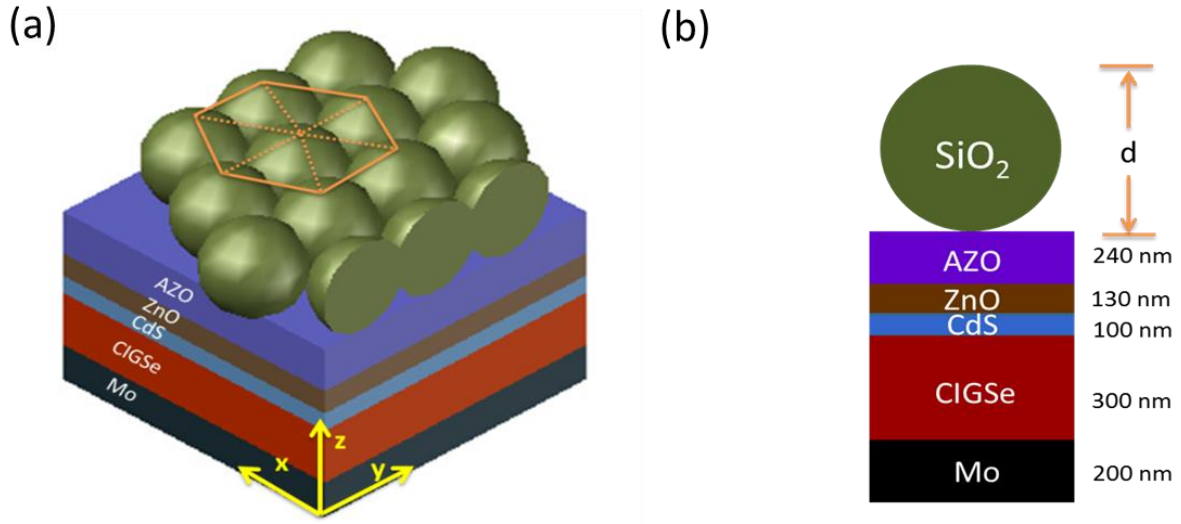

Fig. 1 (a) Schematic illustration of hexagonally closely packed SiO_2 spheres on top of an ultra-thin CIGSe solar cell, (b) corresponding cross section of a single sphere on top

To understand well the absorption enhancement provided by the 2-D SiO_2 nanosphere array on CIGSe solar cells, we performed 3-D simulations with the finite element method (FEM) using the software package JCMsuite [25]. JCMsuite is a commercial FEM solver specialized for nanooptical applications which solves the time harmonic form of Maxwell's equations. Fig. 1(a) illustrates an ultra-thin CIGSe solar cell with hexagonally closely packed SiO_2 spheres on top. The corresponding simulation cross section is presented in Fig. 1(b). The CIGSe solar cell had a typical structure of AZO(Al:ZnO)/ZnO/CdS/CIGSe/Mo from top to bottom. The corresponding thicknesses were 240/130/100/300/200 nm in the simulations presented here. A hexagonal computational domain with three sets of periodic boundary conditions in the *x*-*y* plane and perfectly matched layer boundary conditions in the *z* direction were used. A plane wave source was used incident antiparallel to the z axis, in order to simulate light incident from above the solar cell. To avoid the calculation of point contact between spheres, an approximation of 5% overlap in diameter between neighbouring spheres is assumed. Our simulations have proven that a slight overlap or distance between neighbouring spheres will only lead to minor influence compared to the case of close. The electric field intensity profiles ($|E|^2/|E_0|^2$) in the following images were normalized to the incident electric field intensity ($|E_0|^2$). To calculate the absorption in the layers of the solar

cell, the total field volume integration inside those layers was used. The corresponding photocurrent was obtained by integrating the absorption in the absorber layer multiplied with the solar spectrum and assuming the complete conversion of absorbed photons to collected carriers under standard AM 1.5 illumination condition. To calculate the reflection, the integration of the Poynting flux of the scattered wave leaving the domain in the positive *z* direction was used. The optical constants of each layer were extracted from our own samples via the transfer-matrix method [26]. The refractive index (n) of SiO_2 was set to 1.46 [22]. We should mention here that only the absorption in the CIGSe photoactive layer (Abs_{CIGSe}) can contribute to the photocurrent in the cell [27].

For experimental verifications of the reliability of the simulations, we prepared ultra-thin CIGSe solar cells. Because of the poor electric quality of solar cells with a 300-nm-thick CIGSe layer, the experimental CIGSe layer was 394 nm thick with a Ga/[Ga+In] ratio of 0.35. The thicknesses of the other layers were kept the same as in Fig. 1(b). For solar cell preparation details, please see [28].

The Langmuir-Blodgett method [24] is applied to prepare the 2-D closely packed SiO_2 sphere array due to its simplicity. The colloidal SiO_2 spheres used are commercially available and have no chemical group around the surface. The array preparation starts with suspending the SiO_2 spheres in Butanol, then the SiO_2 suspension is dropped onto the surface of water, in which the solar cells are submerged in a petri dish. SiO_2 spheres spread on the water surface and form a monolayer after Butanol evaporates. Water in the petri dish was subsequently sucked off via an injector until the water level was below the surface of the solar cells. Finally, the result is a 2-D SiO_2 closely packed sphere array on the top of solar cell. In the whole preparation process, the water is the principal liquid medium used and no extra stabilizing agent is needed, which is compatible with the stability of CIGSe solar cells. The area of the petri dish was $5*5cm^2$, but this technology can be easily scaled up to module dimensions.

Scanning electron microscopy (SEM) is used for the characterization of the morphology of SiO_2 nanosphere arrays on top of solar cells. The current density-voltage (J-V) curves were measured under standard test conditions (AM 1.5, 100 mW/cm^2, 25°C) by a home-made system with a sun-simulator consisting of both a Xenon and a Halogen lamp. The AM1.5 condition is calibrated by a certified crystalline Si solar cell. The external quantum efficiency (EQE) was measured with a two-source illumination system of a Xenon and a Halogen lamp, using calibrated Si and Ge diode as references.

3 Results and discussion

3.1 Large sphere array

Whispering gallery modes (WGMs)

Fig. 2(a) represents the simulated absorption in the CIGSe layer (Abs_{CIGSe}) without and with 600-nm-diameter and 110-nm-diameter sphere array. We start the investigation from the big sphere array with a diameter of 600 nm. Though there is an absorption reduction in certain wavelength ranges due to the interference shift, we see an overall enhancement over the whole spectrum of interest for the cell with the 600-nm-diameter sphere array (red dash dotted line) compared to the reference cell without the SiO_2 sphere array (black solid line). In total, this corresponds to a photocurrent improvement of 0.3 mA/cm^2. Remarkably, a sharp and discrete absorption enhancement can be observed around λ = 660 nm. This is ascribed to resonant modes of the periodic sphere array. To further identify it, the electric field intensity profile in the middle of the sphere in the (*x*-*z*) plane is shown in Fig. 2(c). There are two obvious lobes where the electric field is intensified within the sphere. This particular mode pattern has been attributed to Whispering gallery modes (WGMs) [21, 22]. The WGMs act as a cavity for light, trapping it inside the SiO_2 sphere. It can be indicated by the largely reduced reflection R around λ = 660 nm shown in Fig. 2(b). Due to the refractive index of the underlying AZO layer being higher than air, the WGMs have a low Q factor and the confined electric field within SiO_2 spheres preferentially leaks into the underlying solar cell. From the electric field intensity profile in Fig. 2(c), we can observe this leaky effect: the intensity of enhanced electric field is gradually decreasing as it is propagating from the sphere to the solar cell underneath. For comparison, the electric field intensity profile in the (*x*-*z*) plane for a wavelength off resonance (λ = 710 nm) is shown in Fig. 2(d). The electric field concentration inside the sphere is greatly reduced, which leads to less light being coupled towards the underlying solar cell.

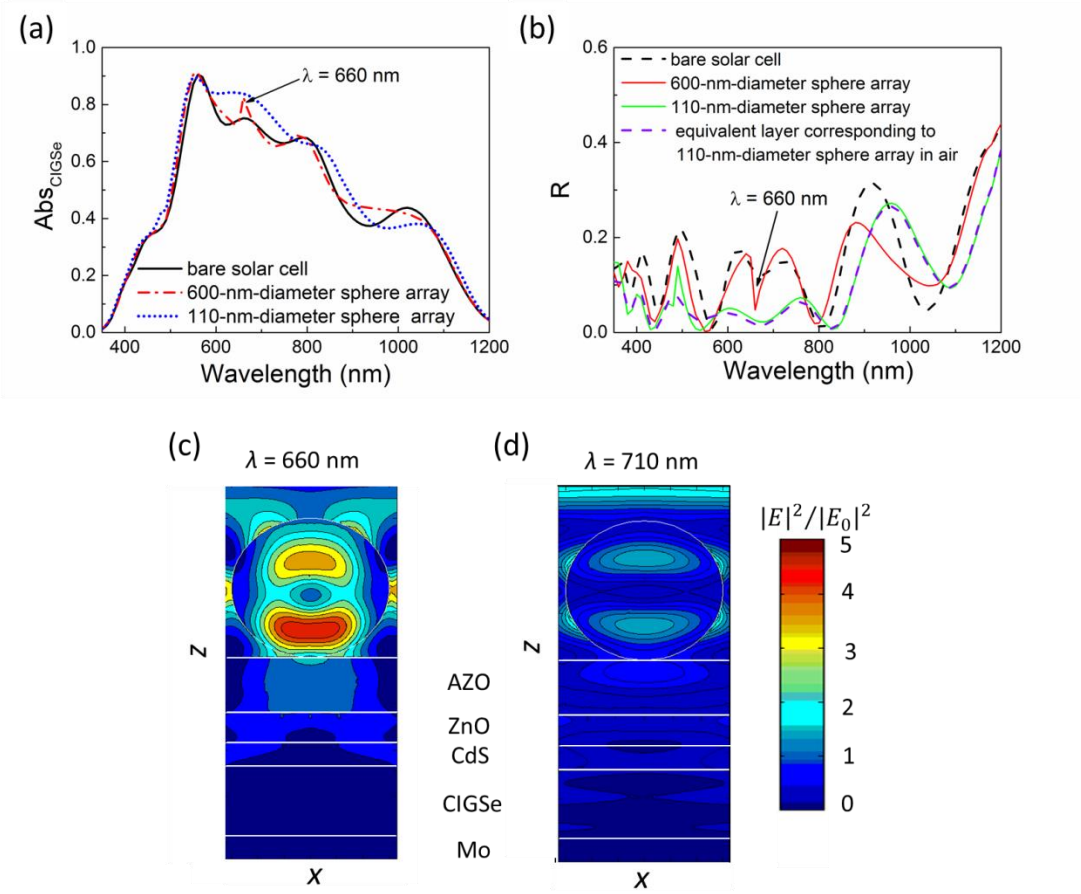

Fig. 2(a) Absorption in the CIGSe layer (Abs_{CIGSe}) and (b) reflection (R) of solar cells with and without a 600-nm-diameter or a 110-nm diameter SiO_2 sphere array; cross sections of electrical field intensity at the middle of the 600-nm-diameter sphere in the (*x*-*z*) plane, (c) at resonance (λ = 660 nm), (d) off resonance (λ = 710 nm)

When the SiO_2 diameter (*d*) varies, the resonance wavelength changes (not shown here). From our simulations, the minimum size of SiO_2 sphere supporting the WGMs in the spectrum of interest (350 -1200 nm) is around 450 nm in diameter.

Higher order multipole Mie resonance

The WGMs, which arise from the total reflection at the internal interface, are unique to the periodic particles with specific shapes like sphere, cylinder and disk [29]. Apart from the WGMs, there are general Mie resonant modes when the nanoparticle size is comparable to the wavelength of the incident light [30, 31]. The near field intensity profiles at λ = 400 and λ =500 nm in Fig. 3(a) and 3(b) confirm the existence of Mie resonances. Mie resonances of spheres were proved to be able to benefit the light absorption in Si solar cells [32]. However, for the 600-nm-dimater spheres, the excitation of higher order multipole (not dipole) resonances mainly lies in the short wavelength range, which is within the parasitic inter-band

absorption range of AZO/ZnO/CdS for CIGSe solar cells (λ < 550 nm). The electric field intensity profiles in Fig. 3(a) and 3(b) imply this. We can observe that the concentrated electric field leaks into the underlying solar cell but it is attenuated completely before reaching the CIGSe layer. This indicates that the corresponding benefit is dissipated by the parasitic absorption in the AZO/ZnO/CdS layers. This observation is in agreement with the corresponding Abs_{CIGSe} and R curves in Fig. 2(a) and 2(b): there is a reduction in R but barely an increase of Abs_{CIGSe} in the range of 400 - 600 nm with the presence of the 600-nm-diameter SiO_2 sphere array on top.

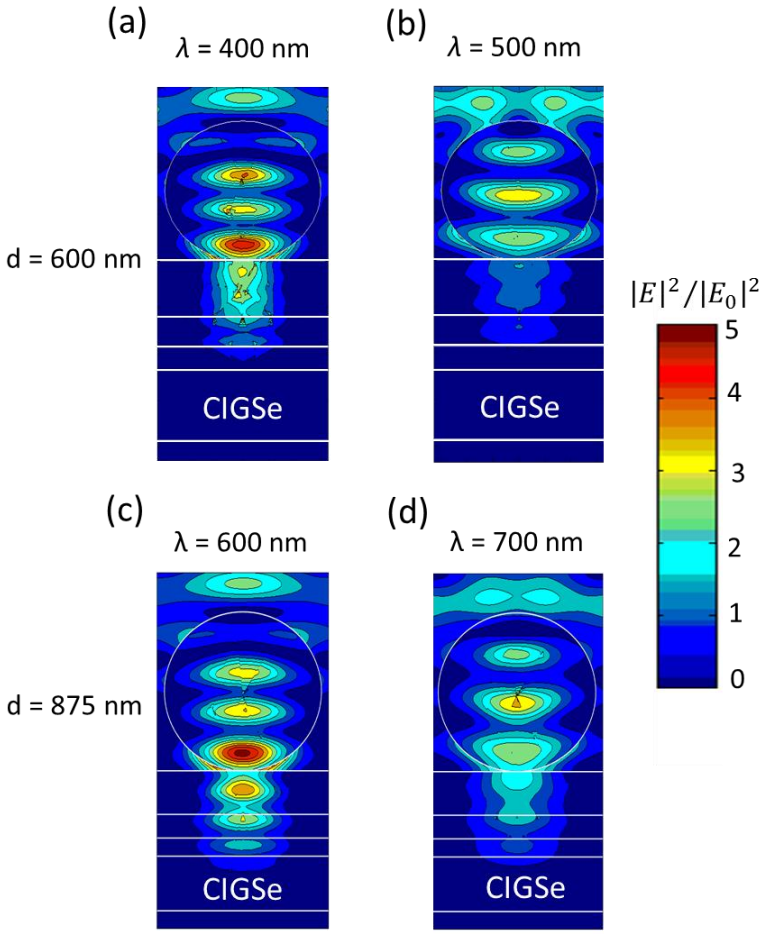

Fig. 3 Cross sections of electric field intensity in the (x-z) plane, at (a) λ = 400 nm, (b) λ = 500 nm for the cell with 600-nm-diameter sphere array; at (c) λ = 600 nm; (d) λ = 700 nm for the cell with the 875-nm-diameter sphere array

When the sphere diameter increases, the multipole Mie resonances can cover a broader spectrum and go beyond the wavelength range of inter band parasitic absorption in the AZO/ZnO/CdS layers. Fig. 3(c) and 3(d) present the electric field intensity profiles of the solar cell with the 875-nm-diameter sphere array. Compared to the case of the 600-nm-

diameter sphere array, the multipole Mie resonances are excited outside the main parasitic range of the AZO/ZnO/CdS layers and the concentrated electric field penetrates into the CIGSe layer. This enhances the absorption in the CIGSe layer. What should be noted here is that only the higher order multipole Mie resonances modes are shown in Fig. 3. The dipole resonance of spheres in principle can also scatter light preferentially into the medium with higher refractive index. However, this beneficial effect was not well pronounced for the sphere array on CIGSe solar cells. The reasons can be interpreted from three factors: 1) The contacting area (point contact) between the sphere and the AZO layer is quite small and the dipole coupling is thus weakened; 2) The effective dipole for the large sphere is far away from the AZO layer and for small spheres the excitation wavelength range is within the parasitic range of AZO/ZnO/CdS layers. Of course, the two factors can suppress the preferential scattering of higher order resonances as well, but the ability of preferential scattering of higher order resonances are less sensitive to the above-mentioned factors than the dipole [31]. This is why we can observe the effect of higher order resonances instead of the dipole.

3.2 Small sphere array

Anti-reflection effect

Fig. 2(a) and 2(b) also present the influence of the small-diameter (d = 110 nm) SiO_2 sphere array on Abs_{CIGSe} and R (dotted line). There is an obvious Abs_{CIGSe} enhancement in a broad spectral range due to the reduction in R. However, the absorption enhancement is mainly ascribed to the closely packed SiO_2 spheres forming an effective anti-reflection layer. To verify this, an effective medium layer with the same thickness as the diameter of the spheres is used. The refractive index of the layer is given by the sum of volume fractions of air and SiO_2 multiplied by their respective refractive indices. This results in an effective refractive index of 1.30. R for the solar cell with this effective layer is simulated (purple dashed line) and compared to that with the corresponding sphere array (blue dotted line) in Fig. 2(b). We find that R from the 3-D simulation assuming spheres on top is quite comparable to that assuming an equivalent layer. Regarding the industrial structure of solar cells imbedded in EVA (n = 1.48), the sphere material should have a refractive index of 1.80 to form an anti-reflection layer between EVA and AZO according to the law $n = \sqrt{n_1 n_2}$, n_1, n_2 are the refractive indexes of EVA and AZO, respectively.

In sum, there are three mechanisms contributing to the light absorption in solar cells depending on the sphere diameter. They are the anti-reflection, WGMs and higher order mutipole Mie resonances. To determine the optimum diameter (*d*) of spheres for Abs_{CIGSe} enhancement, the corresponding photocurrent enhancement is plotted as a function of the diameter of the spheres in Fig. 4. The sphere diameter varies from 40 to 1000 nm. The maximum photocurrent enhancement is reached at the sphere diameter of 110 nm. The 110-nm-diameter small spheres don't support WGMs or higher order multipole resonances, however the broadband anti-reflection effect plays a major role. For the sphere diameter larger than 300 nm, WGMs and multipole Mie resonances dominate the absorption enhancement. WGMs can only be supported in a narrow wavelength range but the multipole Mie resonances can gradually cover the spectral range beyond the main parasitic absorption range of AZO/ZnO/CdS layers as the sphere diameter increases. This explains why the photocurrent density keeps increasing in the diameter range of 300 - 1000 nm. The oscillations originate from the effect of the Fabry-Perot interferences. Nevertheless, the photocurrent enhancement from large sphere arrays is still inferior to that from the optimum anti-reflection effect at the sphere diameter of 110 nm.

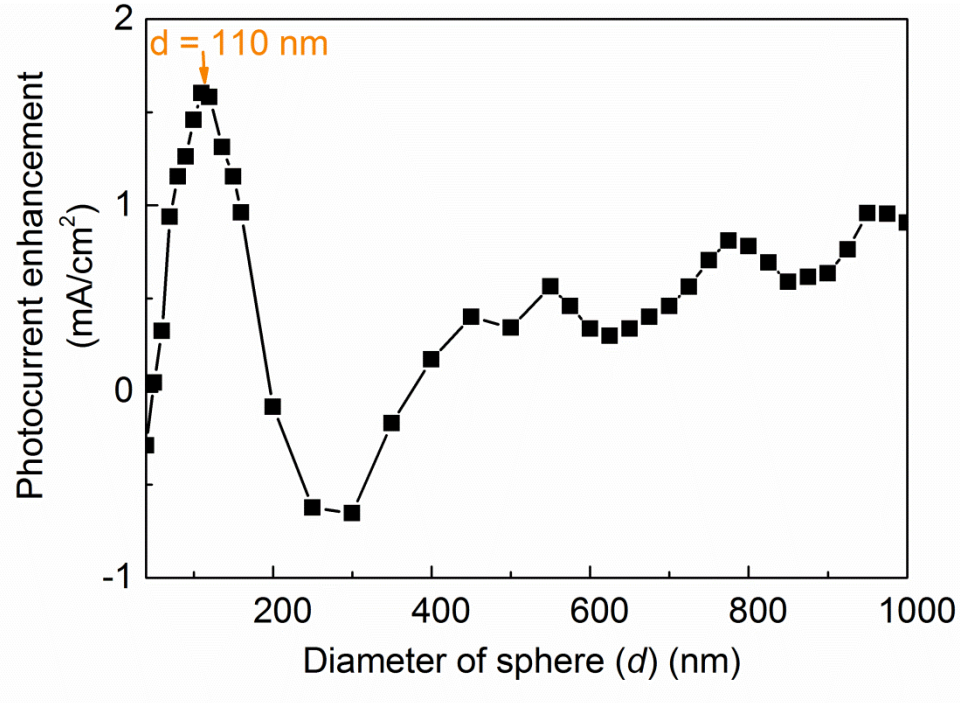

Fig. 4 Photocurrent enhancement of ultra-thin CIGSe solar cell as a function of the size of SiO_2 spheres

3.3 Experimental verification

Fig. 5(a) and 5(b) show the SEM images of the prepared SiO_2 sphere arrays with a sphere diameter of 120 and 600 nm in the top views, respectively. The spheres are generally hexagonally closely packed, though a 5-10 nm distance gap between some spheres is observed mainly due to the influence of surface roughness. This implies that the method we used is a reliable approach to prepare the 2-D closely packed SiO_2 sphere array. Simulations have shown a 5-10 nm gap between spheres will result in minor deviations from the ideally closely packed case. We measured the external quantum efficiency (EQE) curves J-V parameters of solar cells before and after coating the SiO_2 sphere arrays on the same solar cells for each nanosphere size. The results are depicted in Fig. 5 as well as the corresponding simulated Abs_{CIGSe}. The simulated Abs_{CIGSe} is generally higher than the corresponding measured EQE due to incomplete carrier collection in real devices. Interface roughness and thickness deviations will also lead to deviations between the simulated Abs_{CIGSe} and experimentally determined EQE. Nevertheless, the changing trend for the experimental EQE after coating the 2-D sphere array is similar to that for the simulated Abs_{CIGSe} for both sphere sizes. In the case of the 120-nm-diameter sphere array, the enhancement from Abs_{CIGSe} can reach 2.0 mA/cm^2 in terms of photocurrent density Jsc, showing great comparability to the one obtained by integrating from the experimental EQE (1.9 mA/cm^2). The J-V parameters before and after SiO_2 sphere arrays are also shown in Fig. 5(c). After coating the 120-nm-diameter sphere array, J_{sc} increases by 1.6 mA/cm^2. We should note here that only 85-90 % of the solar cell area was coated with the sphere array to prevent coating the front contact grids for electrical measurements. Taking this area factor into account, the J_{sc} increase from J-V measurement is in good agreement with the value integrated from the EQE. Open circuit voltage (V_{oc}) and fill factor (FF) increase slightly, which could be induced by the increase of J_{sc} [33]. As a result, the overall efficiency increases from 9.0% to 9.7% with the presence of the 120-nm-diameter sphere array. For the 600-nm-diameter sphere array, it has little optical benefit on CIGSe solar cells from the Abs_{CIGSe} simulation, which can also be reflected by experimental EQE and J-V measurement.

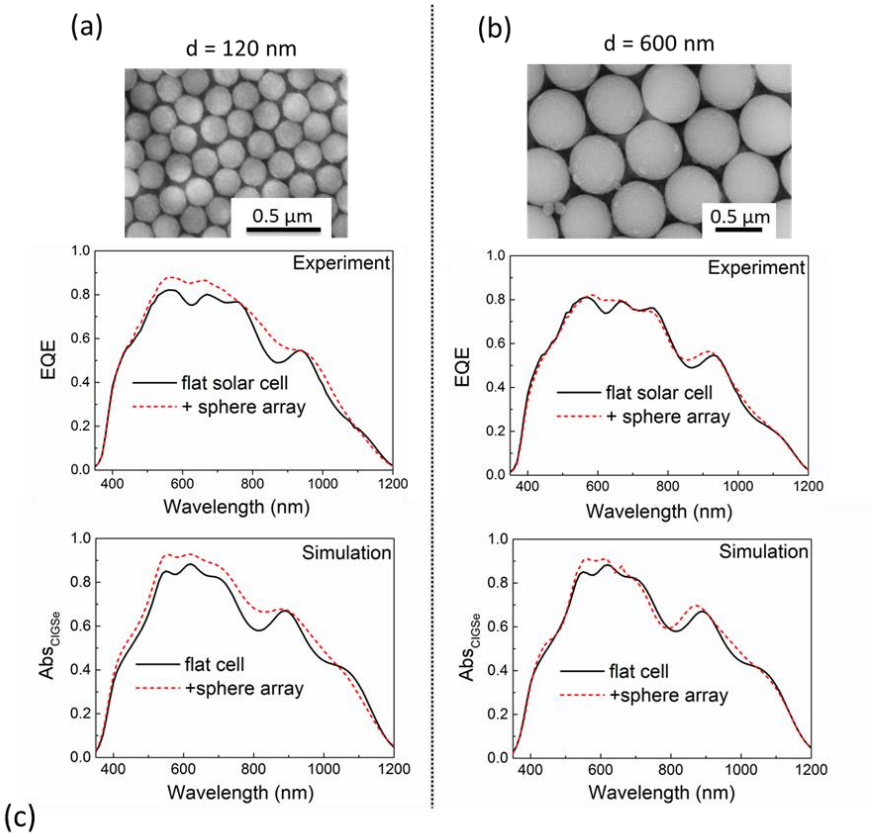

(c)

	V_{oc} (mV)	J_{sc} (mA/cm^2)	FF (%)	Efficiency (%)
bare cells A	537±10	24.2±0.3	69.3±1.5	9.0±0.1
+ 120 nm diameter SiO_2 sphere array	539±10	25.8±0.4	69.6±1.6	9.7±0.1
bare cells B	540±18	24.2±0.2	69.6±2.0	9.1±0.5
+ 600 nm diameter SiO_2 sphere array	540±20	24.6±0.2	69.3±2.4	9.2±0.6

Fig. 5 SEM images of SiO_2 sphere array and comparison of both simulated Abs_{CIGSe} and experimental EQE for the cells without and with the sphere array, (a) sphere diameter d = 120 nm (b) d = 600 nm; (c) J-V parameters with variance error of solar cells before and after closely packed SiO_2 sphere array

3.4 Implication of the closely packed sphere arrays on top of ultra-thin CIGSe solar cells

In Ref. [21, 22], it was discovered for amorphous Si solar cells that a maximum photocurrent enhancement was achieved in the sphere diameter range of 500 - 900 nm due to the presence of WGMs and Mie resonances. This is contrary to the case of the ultra-thin CIGSe solar cells where the optimum absorption enhancement is at the sphere diameter of 110 nm and originates from the anti-reflection effect. This discrepancy is mainly attributed to the structural differences between the two kinds of solar cells: CIGSe solar cells in the simulations and experiments here have three layers (AZO/ZnO/CdS, net thickness 470 nm) on top of the photoactive layer; whereas the amorphous Si cells in Ref. [21, 22] only have one

much thinner ITO ($Sn:In_2O_3$) layer (approx. 100 nm thick). This indicates that the parasitic absorption of light before entering the photoactive layer is much stronger for CIGSe solar cells than for amorphous Si solar cells, especially in the short wavelength range ($\lambda < 550$ nm) where the inter-band absorption in AZO/ZnO/CdS dominates. Additionally, CIGSe solar cells have a Mo back contact, which absorbs the light hitting it rather than reflecting it back. Whereas, for Si solar cells in the references, Ag or TCO/Ag are applied as the back contact which exhibit a high internal reflectivity. This implies that the light trapping effects from the top of cells will be largely dissipated for CIGSe solar cells. Therefore, the effectiveness of absorption enhancement from nanosphere arrays on top of CIGSe solar cells is lower compared to amorphous Si solar cells.

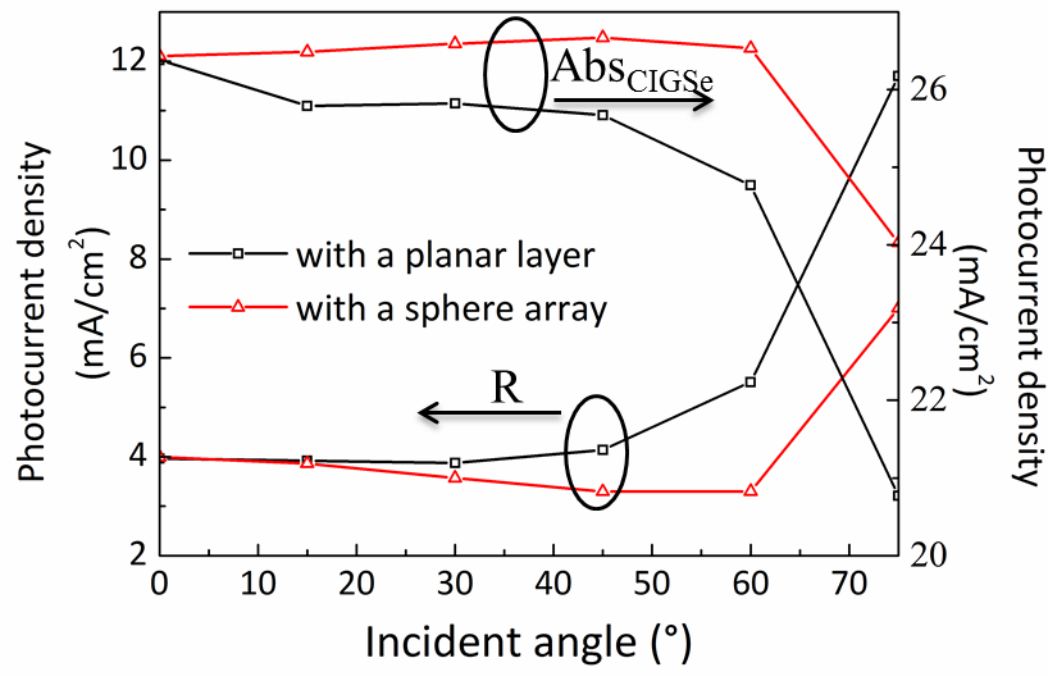

Fig. 6 Dependence of R and Abs_{CIGSe} on incident angle in units of photocurrent density for a 110 nm sphere array and a corresponding effective medium planar anti-reflection coating

Since the effective index of the 110-nm-diameter nanosphere array is similar to that of MgF_2, the optimum anti-reflection effect will be comparable to that of the conventional planar MgF_2 anti-reflection layer with respect to normal incidence. Fig. 6 simulates the angular dependence (0° - 75°) of R and Abs_{CIGSe} in units of photocurrent density for both anti-reflection structures: a 110-nm-diameter-sphere array and a corresponding effective planar layer. For the case of the planar layer, R starts to gradually increase and Abs_{CIGSe} thereby decreases as the incident angle goes up. Whereas for the nanosphere array structure, R actually decreases for angles between 0° - 60° which leads to an increase of Abs_{CIGSe}. At all simulated angles, the

nanosphere array shows a lower R and a resulting higher Abs_{CIGSe} than the planar layer. This implies that the 110-nm-diameter sphere array is a better anti-reflection structure for CIGSe solar cells for oblique incidence.

4. Conclusion

We have both theoretically and experimentally investigated the absorption enhancement of ultra-thin CIGSe solar cells using closely packed SiO_2 sphere arrays. For large spheres, we demonstrated that whispering gallery modes and higher order Mie resonances can enhance the light absorption for the CIGSe cells and dominate the absorption enhancement mechanism. Small spheres were also proved to enhance the light absorption, which is however due to the formation of an effective anti-reflection layer. Compared to amorphous Si solar cells, the maximum absorption enhancement in CIGSe solar cells is achieved for the small sphere array with a diameter of 110 nm rather than big spheres. Experiments confirmed the reliability of our simulations for predicting the influence of the closely packed SiO_2 sphere arrays. Considering the good angular tolerance, the 110-nm-diameter SiO_2 sphere array can be a promising anti-reflection structure for CIGSe solar cells.

Acknowledgements

The authors would like to thank C. Kelch, M. Kirsch and J. Albert for technical support, F. Chu for teaching the preparation of the SiO_2 nanosphere array, C. Xiao for reading the paper. The authors acknowledge the funding from the Helmholtz-Association for Young Investigator groups within the Initiative and Networking fund (VH-NG-928) and G. Yin specially acknowledges the support of funding from China Scholarship Council.

References

1. Z. Jehl, F. Erfurth, N. Naghavi, L. Lombez, I. Gerard, M. Bouttemy, P. Tran-Van, A. Etcheberry, G. Voorwinden, B. Dimmler, W. Wischmann, M. Powalla J. F. Guillemoles, D. Lincot, Thinning of CIGS solar cells. PartII: cell characterizations, *Thin Solid Film* 519(2011) 7212–7215.
2. O. Lundberg, M. Bodegard, J. Malmstrom, L Stolt, Influence of the $Cu(In,Ga)Se_2$ Thickness and Ga Grading on Solar Cell Performance, *Prog. Photovoltaics Res. Appl.* 11(2003) 77-88.

3. M. Gloeckler, J. R. Sites, Potential of submicrometer thickness Cu(In,Ga)Se_2 solar cells, *J. Appl. Phys* 98(2005) 103703.

4. A. Chirilă, S. Buecheler, F. Pianezzi, P. Bloesch, C. Gretener, A. R. Uhl, C. Fella, L. Kranz, J. Perrenoud, S. Seyrling, R. Verma, S. Nishiwaki, Y. E. Romanyuk, G. Bilger, A. N. Tiwari, Highly efficient Cu(In,Ga)Se_2 solar cells grown on flexible polymer films, *Nat. Mater*. 10(2011) 857–861.

5. P. Jackson, D. Hariskos, E. Lotter, S. Paetel, R. Wuerz, R. Menner, W. Wischmann M. Powalla, New world record efficiency for Cu(In,Ga)Se2 thin-film solar cells beyond 20%, *Prog. Photovoltaics Res. Appl.* 19(2011) 894–897

6. B. Vermang, V. Fjällström, J. Pettersson, P. Salomé, M. Edoff, Development of rear surface passivated Cu(In,Ga)Se2 thin film solar cells with nano-sized local rear point contacts, *Sol. Energy Mater. Sol. Cells* 117(2013) 505-11

7. Z. J. Li-kao, N. Naghavi, F. Erfurth, J. F. Guillemoles, I. Gérard, A. Etcheberry, J. L. Pelouard, S. Collin, G. Voorwinden, D. Lincot, Towards ultrathin copper indium gallium diselenide solar cells: proof of concept study by chemical etching and gold back contact engineering, *Prog. Photovoltaics Res. Appl.* 20(2012), 582–587.

8. H. Tan, R. Santbergen, A. H. M. Smets, and M. Zeman, Plasmonic Light Trapping in Thin-film Silicon Solar Cells with Improved Self-Assembled Silver Nanoparticles," *Nano Let.* 12(2012).

9. H. Atwater, A. Polman, Plasmonics for improved photovoltaic devices, *Nat. Mater*. 9(2010), 205–213.

10. N. P. Hylton, X. F. Li, V. Giannini, K.-H. Lee, N. J. Ekins-Daukes, J. Loo, D. Vercruysse, P. Van Dorpe, H. Sodabanlu, M. Sugiyama, and S. a Maier, Loss mitigation in plasmonic solar cells: aluminium nanoparticles for broadband photocurrent enhancements in GaAs photodiodes, *Sci. Rep.* 3(2013), 2874.

11. W. Ren, G. Zhang, Y. Wu, H. Ding, Q. Shen, K. Zhang, J. Li, N. Pan, X. Wang, Broadband absorption enhancement achieved by optical layer mediated plasmonic solar cell, *Opt. Express* 19(2011), 26536–26550.

12. E. Wang, S. Mokkapati, T. P. White, T. Soderstrom, S. Varlamov, K. R. Catchpole, Light trapping with titanium dioxide diffraction gratings fabricated by nanoimprinting, *Prog. Photovoltaics Res. Appl.* 22(2014), 587–592.

13. T. K. Chong, J. Wilson, S. Mokkapati, K. R. Catchpole, Optimal wavelength scale diffraction gratings for light trapping in solar cells, *J. Opt.*, 14(2012) 024012.

14. D. Zhou, R. Biswas, Photonic crystal enhanced light-trapping in thin film solar cells, *J. Appl. Phys.* 103(9), 093102 (2008).

15. Y. Yao, J. Yao, V. K. Narasimhan, Z. Ruan, C. Xie, S. Fan, and Y. Cui, Broadband light management using low-Q whispering gallery modes in spherical nanoshells, *Nat. Commun.* 3(2012), 664.

16. M. Schmid, R. Klenk, M. C. Lux-Steiner, M. Topic, J. Krc, Modeling plasmonic scattering combined with thin-film optics, *Nanotechnology* 22(2011), 025204.

17. C. Colin, I. Massiot, A. Cattoni, N. Vandamme, C. Dupuis, N. Bardou, I. Gerard, N. Naghavi, J.-F. Guillemoles, J.-L. Pelouard, S. Collin, Broadband light-trapping in ultra-thin nano-structured solar cells, *Proc. SPIE* 8620(2013), 86200C.

18. W. Wang, S. Wu, R. J. Knize, K. Reinhardt, Y. Lu, S. Chen, Enhanced Photon Absorption and Carrier Generation in Nanowire Solar Cells, *Opt. Express* 20(2012), 3733–3743.

19. Y. Li, B. Qian, C. Li, J. Xu, C. Jiang, Optical properties of nanocrystal-silicon thin films on silicon nanopillar arrays after thermal annealing, *Appl. Surf. Sci.* 265(2013), 324– 328

20. W. Kandulski, Shadow Nanosphere Lithography, dissertation, University of Bonn, Germany, (2007)

21. J. Grandidier, D. M. Callahan, J. N. Munday, H. A. Atwater, Light Absorption Enhancement in Thin-Film Solar Cells Using Whispering Gallery Modes in Dielectric Nanospheres, *Adv. Mater.* 23(2011), 1272–1276.

22. J. Grandidier, R. a. Weitekamp, M. G. Deceglie, D. M. Callahan, C. Battaglia, C. R. Bukowsky, C. Ballif, R. H. Grubbs, H. A. Atwater, Solar cell efficiency enhancement via light trapping in printable resonant dielectric nanosphere arrays, *Phys. Status Solidi* 210(2013), 255–260.

23. Y. Zhang, T. Wei, J. Wang, C. Fan, Y. Chen, Q. Hu, J. Li, Efficiency improvement of InGaN light emitting diodes with embedded self-assembled SiO_2 nanosphere arrays, *J. Cryst. Growth* 394(2014),7–10

24. G. D. Moon, T. Il Lee, B. Kim, G. Chae, J. Kim, S. Kim, J.-M. Myoung, and U. Jeong, Assembled Monolayers of Hydrophilic Particles on Water Surfaces, *ACS Nano*, 5(2011) 8600–8612.

25. J. Pomplun, S. Burger, L. Zschiedrich, F. Schmidt, Adaptive finite element method for simulation of optical nano structures, *Phys. Stat. Sol. (b)* 244(2007) 3419-34.

26. G. Yin, C. Merschjann, M. Schmid, The effect of surface roughness on the determination of optical constants of $CuInSe_2$ and $CuGaSe_2$ thin films, *J. Appl. Phys*. 113(2013) 213510.

27. R. Klenk, Characterization and modelling of chalcopyrite solar cells, *Thin solid films* 387(2001), 135–140.

28. G. Yin, V. Brackmann, V. Hoffmann, M. Schmid, Enhanced performance of ultra-thin $Cu(In,Ga)Se_2$ solar cells deposited at low process temperature, *Sol. Energy Mater. Sol.* Cells, 132(2015) 142–147.

29. A. N. Oraevsky, Whispering-gallery waves, *Quantum Electron*. 32(2002), 377–400.

30. Bohren CF, Huffman DR: Absorption and scattering of light by small particles. New York: Wiley; 1983.

31. M. Schmid, P. Andrae, P. Manley, Plasmonic and photonic scattering and near fields of nanoparticles, *Nanoscale Res. Lett.* 9(2014), 50.

32. C. R. Simovski, A. S. Shalin, P. M. Voroshilov, P. A. Belov, Photovoltaic absorption enhancement in thin-film solar cells by non-resonant beam collimation by submicron dielectric particles, *J. Appl. Phys.* 114(2013), 103104.

33. C. van Lare, G. Yin, A. Polman, M. Schmid, Light Coupling and Trapping in Ultrathin Cu(In,Ga)Se_2 Solar Cells Using Dielectric Scattering Patterns, *ACS Nano* 9(2015), 9603